Doctor of Philosophy

In vivo Analysis of Optic Nerve in an Elderly Population Using Diffusion Magnetic Resonance Imaging Tractography

The Graduate School

of the University of Ulsan

Department of Medicine

Yeji Moon

In vivo Analysis of Optic Nerve in an Elderly Population Using Diffusion Magnetic Resonance Imaging Tractography

Supervisor: Hyun Taek Lim

A Dissertation

Submitted to

the Graduate School of the University of Ulsan

In partial Fulfillment of the Requirements

For the Degree of

Doctor of Philosophy

by

Yeji Moon

Department of Medicine

University of Ulsan, Korea

February 2021

In vivo Analysis of Optic Nerve in an Elderly Population Using Diffusion Magnetic Resonance Imaging Tractography

This certifies that the dissertation

of Yeji Moon is approved.

Hyosook Ahn

Committee Chair Dr.

Hyun Taek Lim

Committee Member Dr.

Jae Yong Kim

Committee Member Dr.

Joo Yong Lee

Committee Member Dr.

Han Woong Lim

Committee Member Dr.

Department of Medicine

University of Ulsan, Korea

February 2021

Abstract

Purpose: To quantitatively investigate the microstructural properties of the optic nerve (ON) *in vivo* using diffusion magnetic resonance imaging (dMRI) tractography in an elderly population and to determine the differences between the ON diffusion properties stratified by basic demographics

Methods: We measured fractional anisotropy (FA), mean diffusivity (MD), radial diffusivity (RD) and axial diffusivity (AD) of the intraorbital ON in cognitively normal controls selected from the Alzheimer's Disease Neuroimaging Initiative 3 database (n = 132, mean age 74.5 ± 8.2 years) using dMRI probabilistic tractography and evaluated the correlation between diffusion parameters and demographic factors. Diffusion parameters were measured in 20 equidistant nodes along the tract.

Results: The mean FA of the entire intraorbital ON was 0.346 ± 0.078 and the mean MD was 1.266 ± 0.196 $\mu m^2/s$. The mean RD was 1.009 ± 0.195 $\mu m^2/s$ and the mean AD was 1.764 ± 0.210 $\mu m^2/s$. FA gradually increased from 0.250 to 0.404 toward the orbital apex, whereas MD, RD and AD decreased from 1.529 to 1.121 $\mu m^2/s$, from 1.323 to 0.851 $\mu m^2/s$, and from 1.950 to 1.659 $\mu m^2/s$, respectively. The multiple linear regression model showed a negative correlation between FA and age in all 20 nodes, and FA in females was significantly higher thant males. However, MD showed no significant correlation with age, and the MD of the anterior 19 nodes correlated with sex. Females had significantly lower RD in all nodes of the intraorbital ON, and RD was correlated with age in a fourth of the ON. Meanwhile, no variable was entered into the multiple linear regression model by a stepwise entry for AD except for the first node.

Conclusions: We measured the diffusion properties along the intraorbital ON using dMRI tractography in an elderly cognitively normal population. FA had an inverse relationship with MD, where the FA gradually decreased with age and toward the eye globe, and the MD showed the opposite trend. Females had higher FA and lower MD and RD than males. The diffusion properties detected by dMRI tractography may substantially reflect the microstructure of the ON.

Index

Introduction

The optic nerve (ON) is formed by the convergence of 1.2 million retinal ganglion cell axons and it is the pathway which transfers the visual information from the retina to the visual cortex. It is the second cranial nerve and considered as a part of the central nervous system as it extends from the diencephalon during embryonic development. Therefore, the retinal nerve fiber and ON have been studied as a surrogate for various neurodegenerative diseases such as Alzheimer's disease and Parkinson's disease.[1, 2]

Optical coherence tomography (OCT), one of the most commonly used imaging techniques in ophthalmology, provides *in vivo* images of the retina and ON with high resolution (< 10 μm).[3, 4] However, it has several limitations, and the most significant is the penetration depth. OCT can hardly show deep structures beyond the sclera, such as the retrobulbar ON.[5, 6]

Meanwhile, magnetic resonance imaging (MRI) shows structural changes throughout the ON, and diffusion MRI (dMRI), which creates images based on the relative diffusion of water molecules in the tissue, is sensitive to microstructural changes in the brain white matter. Recently dMRI has emerged as a useful tool to investigate the structure of nervous tissues at a microscopic level, although the resolution of images is a millimetric scale. It has the potential to provide information of the cellular organization of nervous tissues noninvasively and *in vivo*. Moreover, dMRI has been used to monitor the dynamic changes during neuronal activation, which suggests that it could perform as a functional neuroimaging modality.

Based on dMRI, diffusion tensor imaging (DTI) investigates the fiber architectures of several organs in human body, such as the brain white matter or cardiac muscle fibers. The white matter and cranial nerves including the ON consist of bundles of axons. The axon membranes and myelin sheaths

mainly induce diffusion restriction of water molecules. The direction of maximum diffusivity become parallel to the axonal direction, making the diffusion anisotropic.[7, 8] Under the anisotropic condition, the probable location of a molecule after a certain time will be within an ellipsoid. DTI techniques were acquired using this ellipsoid shaped mathematical model. The ellipsoid can be characterized by three vectors (ε_1, ε_2, ε_3) called the eigenvectors, with corresponding lengths (λ_1, λ_2, λ_3), the eigenvalues. (Figure 1) The eigenvectors and eigenvalues describe the shape of the ellipsoid and the relationship between the principal coordinate axes in three-dimensional space.

Figure 1. Visual presentation of the diffusion tensor model. The ellipsoid shaped area of a water molecule diffusion can be characterized by three eigenvectors (ε_1, ε_2, ε_3) and three eigenvalues (λ_1, λ_2, λ_3).

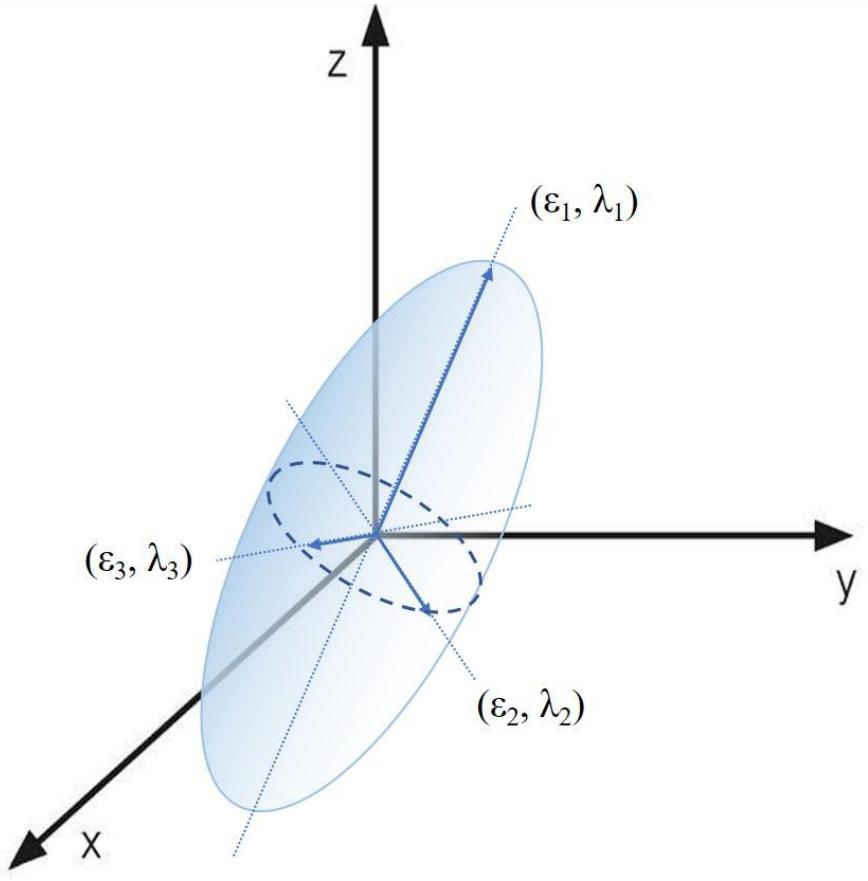

The three-dimensional reconstruction of nerve fiber tracts of DTI data is called tractography. The global architectures of fiber bundles are reconstructed by connecting the local information in voxels. There are two major approaches in tractography: deterministic and probabilistic tractography.[9, 10] With deterministic tractography, the tract begins from a seed point and traces along the most likely direction. (Figure 2(A)) The major eigenvectors of the diffusion tensor represent the final fiber vector. However, when DTI is ambiguous and cannot accurately describe the fiber direction in some complex regions, this tractography is prone to substantial errors.

Meanwhile, probabilistic tractography was proposed to address the reliability of deterministic tractography. Probabilistic fiber-tracking methods generate a large collection of possible trajectories from each seed point by repeating the streamlining process multiple times. (Figure 2(B)) Given the capabilities and ambiguities of dMRI of today, probabilistic tractography provides more complete information than deterministic tractography. However, probabilistic tractography is computationally more expensive compared with deterministic tractography.[11]

Figure 2. Schematic figures showing the differences between (A) deterministic tractography and (B) probabilistic tractography. In deterministic approach for tractography, the tract begins from a seed point (blue) and traces along the most likely direction. On the other hand, probabilistic approaches generate a large collection of possible fibers. Probabilistic approaches are more extensive and computationally demanding because they track all orientations in all voxels adjacent to the seed point.

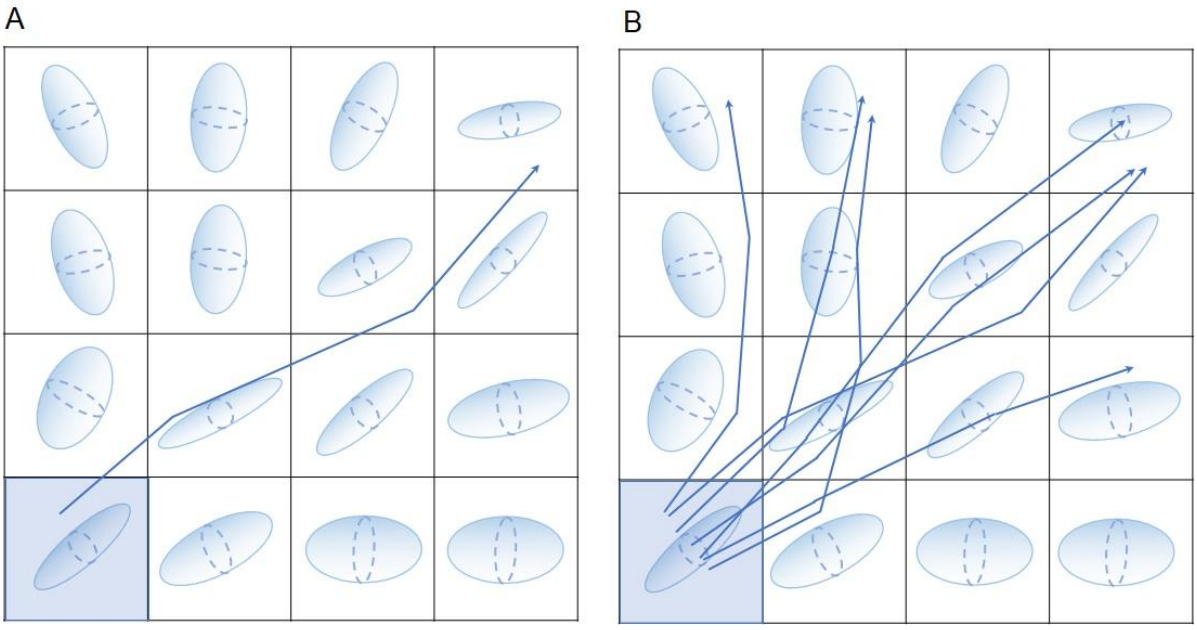

The most commonly used diffusion parameters in DTI are fractional anisotropy (FA) and mean diffusivity (MD).[12-14] FA is the normalized standard deviation of the three eigenvalues. Its value characterizes the fraction of molecular displacements ranging from 0 for completely isotropic diffusion to 1 for completely anisotropic diffusion. FA represents the directionality of diffusion, independently of the rate of diffusion. Although FA is highly sensitive to microstructural changes, it is not specific to each type of microstructural changes. Therefore, it is desirable to include other DTI measurements, such as MD, in any analysis. MD is the mean of three eigenvalues, and it is a measure of the ellipsoid volume as the overall mean displacement of water molecules. Thus, it reflects the mean amount of diffusion, irrespective of the direction of diffusion. MD is sensitive to cellularity, edema, and necrosis.

The apparent diffusivity is also measured as radial diffusivity (RD) or axial diffusivity (AD). RD is the apparent water diffusion in the direction perpendicular to the axonal fibers, whereas AD refers to the diffusivity along the main axis which is defined as the magnitude of water diffusion parallel to the

axonal fibers. RD and AD represent the eigenvalue amplitudes and demonstrate more specific relationships to pathologic changes.[15] RD has been related to the degree of myelination, although axonal diameters or density may also influence RD. In contrast to RD, AD has been assumed to represent the axonal integrity.[16, 17] In general, higher FA in nerve fibers have been reported to link to preserved fiber integrity, whereas increases in MD and RD to be related to the structural disruption of nervous tissues.[18]

Although one diffusion parameter may be highly correlated with a certain type of microstructural alterations, it seems necessary to consider various diffusion parameters together to differentiate the pathologic changes. Adding RD and AD helps understanding which component of the diffusion tensor contribute to changes of MD and FA. For instance, FA can decrease as a result of an increase in RD or a decrease in AD. Conversely, we would not know whether the change of AD or RD is significant enough to affect the anisotropy or the overall diffusivity by measuring only AD and RD. It is advantageous to consider all four parameters when investigating the diffusion properties of nervous fibers.

It has been difficult to investigate ON microstructure using dMRI because the ON is a small structure with respect to the resolution of dMRI and surrounding tissues such as nasal cavity induce artifacts in the MR signal. In addition, previous studies that used dMRI to evaluate ON changes in various diseases have measured the diffusion parameters in regions of interest (ROIs).[19-21] Therefore, they only measured the diffusion in small portions of the ON, not in its full extent. However, recent advancements in dMRI scanning and preprocessing protocols have reduced various artifacts, and probabilistic tractography can longitudinally visualize the neural tracts that are not confined to the ROIs.[22-24]

Although several reports have suggested the usefulness of probabilistic tractography for evaluating ON, these studies had limitations, including a small number of subjects, and little has reported normal values of dMRI parameters for ON.[25, 26] For the standard implementation of dMRI for ON evaluation, it is required to investigate the normal values of these parameters. It is particularly essential to assess the microstructural properties of ON and to determine reference values of diffusion parameters in detail for an aged population who are susceptible to neurodegenerative changes.

In this study, we aimed to quantitatively investigate *in vivo* ON diffusion properties using dMRI probabilistic tractography in an elderly population. Furthermore, we intended to determine the differences between the ON diffusion properties stratified by basic demographics. We are to measure RD and AD as well as FA and MD to verify the changes in diffusion properties more specifically and to assess clinical applicability of each diffusion parameter in dMRI.

Methods

Subjects

The MRI data used in this study were obtained from the database of the third phase of the Alzheimer's Disease Neuroimaging Initiative (ADNI3; http://adni.loni.usc.edu). The ADNI3 data were collected for more than 300 participants using new dMRI protocols for all GE, Siemens, and Philips scanners at 47 sites across the United States and Canada. ADNI data are publicly available, and they have been used in by various studies. [27, 28]

ADNI research activities were reviewed and approved by the Institutional Review Board (IRBs) of each participating facility, and written informed consent was obtained from each participant. This study was exempted from IRB approval because it involved a secondary analysis of de-identified ADNI data.

Each subject was scanned during two or more visits, separated by at least 6 months, and ADNI3 is still ongoing. We selected normal controls who underwent only Siemens 3 Tesla MRI (Basic Skyra E11 and Prisma D13; Siemens, Erlangen, Germany) to collect the largest cohort of normal patients with a wide age range and avoid different scan acquisition parameters, including vendor, voxel size, and angular resolution, known as the scanner effect on diffusion measures.[29-32]

Of 144 normal controls one subject was excluded because he showed high signal intensity for his left eye on T1-weighted MR images, and other 11 subjects were excluded because of failure of image processing; 132 of the final were included.

Magnetic Resonance Images Acquisition

As mentioned above, all subjects underwent Siemens 3 Tesla MRI (Basic Skyra E11 and Prisma D13; Siemens, Erlangen, Germany). T1-weighted anatomical images were obtained using an MPRAGE sequence with a 1 × 1 × 1 mm voxel size and a 2300-ms repetition time (TR). For diffusion-weighted MRI, the pulse sequence was acquired in the axial plane (56 ms echo time (TE); 7200 ms TR; two b-values with b = 0 and b = 1000 s/mm^2; 48 diffusion directions, 7 non-diffusion weighted images, 2 × 2 × 2 mm voxel size). Further details on scan parameters can be found in https://adni.loni.usc.edu/wp-content/uploads/2017/07/ADNI3-MRI-protocols.pdf.

Image Preprocessing

DTI data were preprocessed for denoising and bias field correction using MRtrix3 software package (http://www.mrtrix.org) based on previously published methods.[33-37] MRtrix3 is a software platform for medical image processing, analysis, and visualization. It was developed for the investigation of the brain white matter using dMRI. It is implemented using a lightweight framework for image data access and manipulation.

Subsequent processing was performed using the mrDiffusion software package (https://github.com/vistalab/vistasoft). The anatomical T1-weighed images were aligned to the anterior commissure–posterior commissure plane. Diffusion-weighted images were corrected for eddy currents and subject motions by a 14-parameter constrained nonlinear coregistration based on the expected pattern of eddy-current distortions given the phase-encode direction of the acquired data.[38] The motion-corrected non-diffusion-weighted (b0) images were averaged and aligned to the structural T1-weighted images using a rigid body mutual information algorithm. Diffusion-weighted images were registered to the mean of the motion-corrected b0 images using a two-stage coarse-to-fine approach that maximized

the normalized mutual information. Diffusion-weighting gradient directions were reoriented by applying the same transformation used on the diffusion-weighted images.

All images from the diffusion sequence were resampled to 2-mm isotropic voxels using a trilinear interpolation algorithm based on code from statistical mapping software (SPM8; http://www.fil.ion.ucl.ac.uk/spm/). The rotation component of the omnibus coordinate transform was applied also to the diffusion-weighting gradient directions to preserve their orientation with respect to the resampled diffusion images. Finally, the tensors were optimized for estimation using a least-squares algorithm with bootstrapping for 500 times.

Regions of Interest for Fiber Tractography

We manually identified two ROIs for each intraorbital ON. To identify the starting point for the ON, we placed a 4-mm radius spherical ROI just posterior to the globe of each eye and centered on the emerging ON. (Figure 3(A)) Another 4-mm radius spherical ROI was placed in the orbital apex and its center was placed in the center of the annulus of Zinn, where the extraocular muscles were confluent. (Figure 3(B)) The diameter of the ROIs was larger than those of the ONs of the participants to prevent undersampling at the tractography stage.

The placement of ROIs was based on the gross anatomical landmarks in the T1-weighted and b0 images. When there was a difference between the locations of the ROIs of the T1-weighted and b0 images, we choose b0 images to locate the ROI. A single author (Y.M.) defined ROIs for each subject in randomized and blinded manner.

Figure 3. Regions of Interest placement for fiber tractography. (A) Axial and sagittal views (top to bottom) of the regions of interest (ROIs). A 4-mm radius spherical ROI just posterior to the globe was centered on the emerging optic nerve in each eye. (B) Another 4-mm radius spherical ROI was within the orbital apex and its center was placed in the center of the annulus of Zinn. Visualization of the ROIs was generated with the Matlab Brain Anatomy software package (https://github.com/francopestilli/mba).

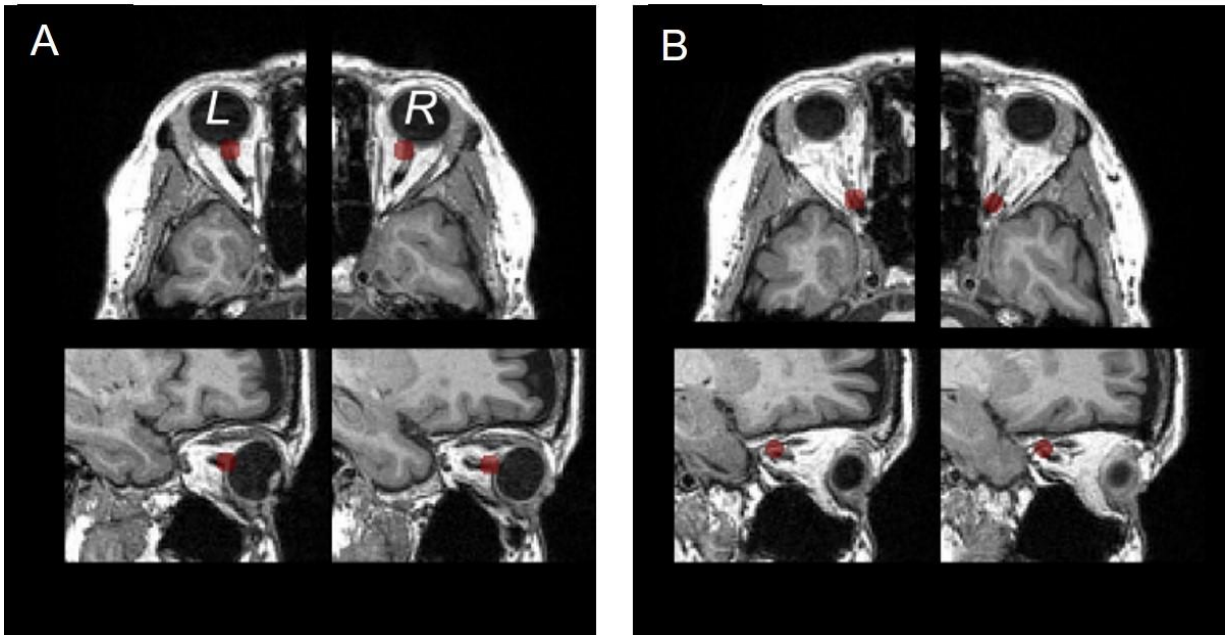

Fiber Tracking and Cleaning

The ON was identified using probabilistic fiber tractography to calculate the most likely pathway between a pair of ROIs using ConTrack (https://github.com/vistalab/contrack). This tool was used to identify visual pathways in previous studies.[39, 40] ConTrack comprises three stages. In first stage, it generates a large set of potential pathways. Next, a scoring algorithm measures the likelihood of a pathway. Finally, in the inferential step, it identifies the most likely pathways connecting two ROIs. In this study, the most likely pathway was generated from a set of 1000 candidate pathways between the

ON head and orbital apex. The ConTrack scoring algorithm was used to select the 100 most likely fibers (top 10%). (Figure 4(A))

A fiber was automatically removed when its distance was more than 2.4 standard deviation away from the pathway's fiber core or more than 3 standard deviation longer than the average fiber length, following the prescriptions of a previous study.[26] Fiber cleaning was performed using the Automated Fiber Quantification (AFQ) toolkit (Stanford University, https://github.com/jyeatman/AFQ). The pathways of all participants were processed using the same AFQ cleaning parameters. (Figure 4(B))

Figure 4. Fiber tracking and cleaning. (A) One hundred most likely fibers were selected using ConTrack scoring algorithm. (B) After automatic cleaning process using Automated Fiber Quantification toolkit, 53 fibers were remained.

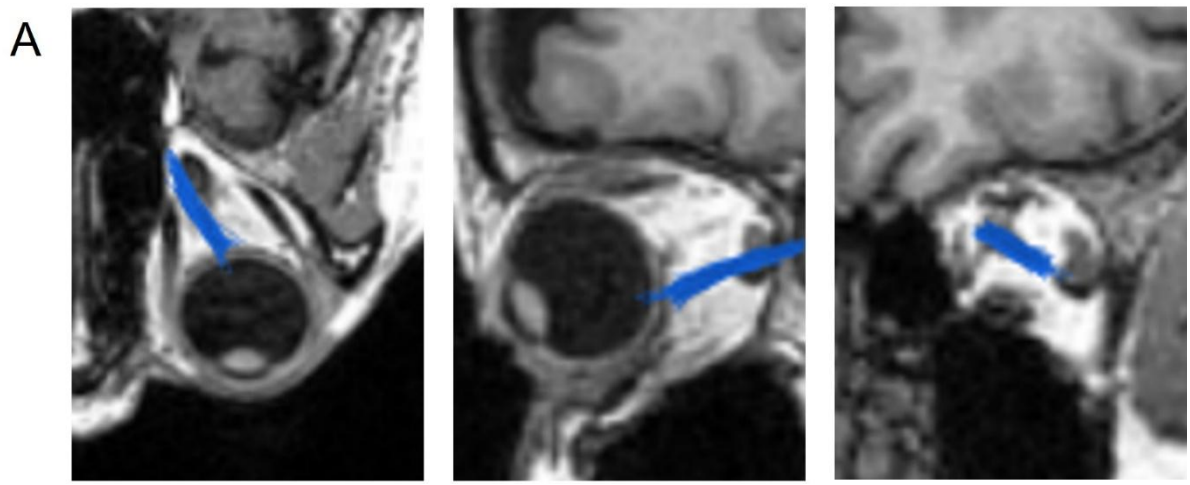

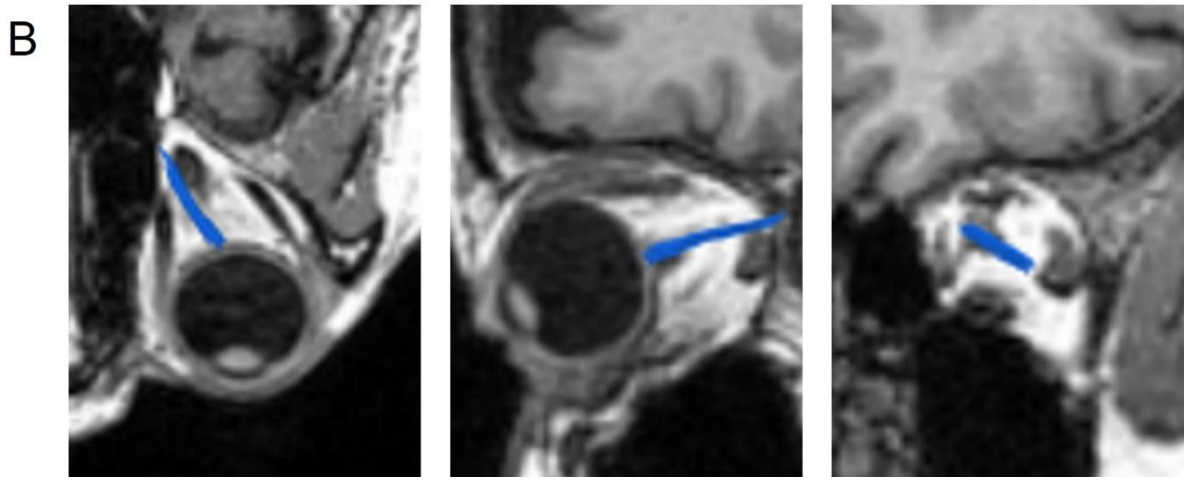

After automated cleaning, all the ON pathways were subjected to quality assessment, and additional manual cleaning was applied as necessary by a single author (Y.M.) in randomized and blinded manner. Fibers were overlaid on the anatomical T1 volume and any fibers that were found to be anatomically implausible were manually removed. (Figure 5)

Figure 5. Tractography using diffusion magnetic resonance imaging. This shows the cleaned tractography-generated optic nerve pathways (red fibers for left optic nerve and blue fibers for right optic nerve) Visualization of the tractography was generated with the Matlab Brain Anatomy software package (https://github.com/ francopestilli/mba).

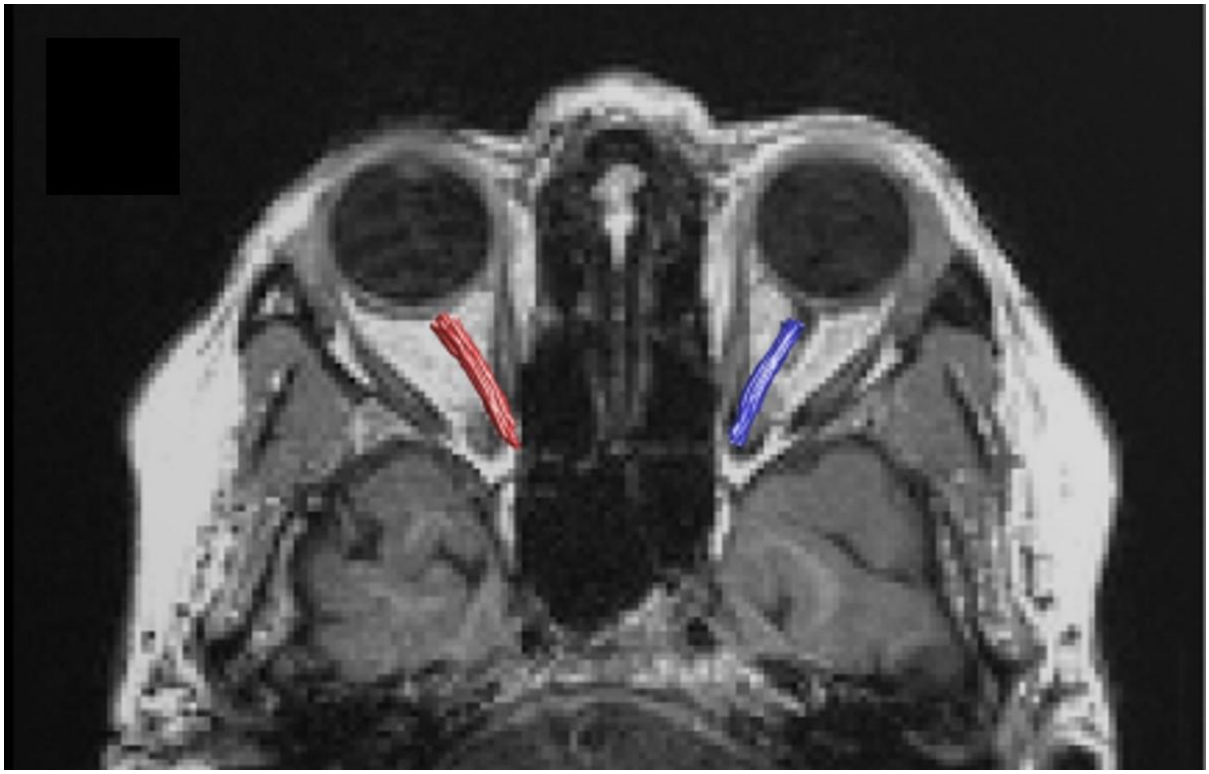

Diffusion Measures Based on Tractography

Voxel-wise tensor properties were extracted from the volumetric region in the tractography-generated pathway. The resulting eigenvalues were used to compute diffusion properties.[41] The main diffusion parameters calculated in this study were FA, MD, RD and AD.

The following formulae were used for each diffusion parameter:

$$FA = \sqrt{\frac{(\lambda_1 - \lambda_2)^2 + (\lambda_2 - \lambda_3)^2 + (\lambda_3 - \lambda_1)^2}{2((\lambda_1)^2 + (\lambda_2)^2 + (\lambda_3)^2)}}$$

$$MD = \frac{(\lambda_1 + \lambda_2 + \lambda_3)}{3}$$

$$RD = \frac{(\lambda_2 + \lambda_3)}{2}$$

$$AD = \lambda_1$$

We measured the diffusion properties in each 20 equidistant nodes along the ON to normalize the pathway length and facilitate statistical analysis. The values for diffusion properties were generated for each node using a Gaussian-weighted average, where the central tract was weighted over the outlying fibers. We averaged across these samples to measure single-value summaries of the entire ON pathway. Additionally, 100 samples were taken at 100 equidistant positions along the ON length to visualize tract profiles for diffusion parameters. (Figure 6) This approach has been described in detail in previous studies.[25, 26, 42]

Figure 6. Visualization of diffusion properties diffusion magnetic resonance imaging tractography. Profiles of (A) fractional anisotropy and (B) mean diffusivity ($\mu m^2/s$) are represented by the colored cylinders.

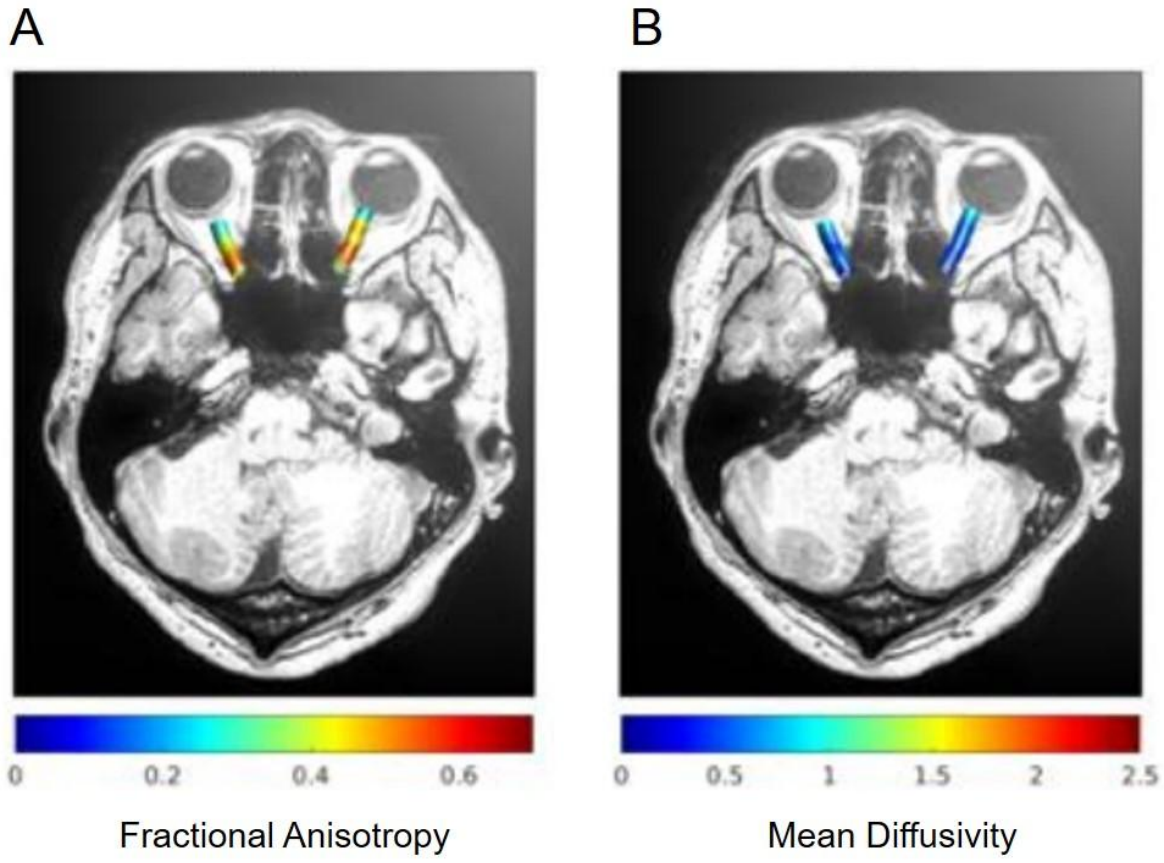

Statistical Analysis

The procedures from ROIs placement to diffusion measurement were performed twice independently, from which the mean values of diffusion parameters were obtained. The intraclass coefficient (ICC) value of the parameters were summarized in Table 1.

Table 1. Intraclass correlation coefficient of diffusion parameters.

Node[a]	Fractional anisotropy	Mean diffusivity	Radial diffusivity	Axial diffusivity
1	0.898	0.906	0.897	0.914
2	0.907	0.915	0.910	0.917
3	0.911	0.912	0.916	0.912
4	0.917	0.900	0.914	0.900
5	0.922	0.895	0.910	0.892
6	0.932	0.900	0.906	0.886
7	0.937	0.906	0.900	0.881
8	0.934	0.908	0.896	0.877
9	0.932	0.909	0.892	0.872
10	0.927	0.908	0.894	0.867
11	0.924	0.907	0.905	0.865
12	0.928	0.904	0.919	0.865
13	0.935	0.902	0.931	0.860
14	0.941	0.904	0.936	0.854
15	0.944	0.909	0.937	0.853
16	0.943	0.915	0.935	0.863
17	0.944	0.921	0.932	0.877
18	0.942	0.921	0.927	0.880
19	0.936	0.912	0.925	0.881
20	0.927	0.904	0.928	0.888

[a]The nodes of each optic nerve were numbered from the optic nerve head to the orbital apex.
All intraclass correlation coefficients are statistically significant ($p < 0.001$).

Strong correlation between right and left eye diffusion parameters were observed (FA, Pearson correlation coefficient = 0.778, $p < 0.001$, MD Pearson correlation coefficient = 0.702, $p < 0.001$, RD Pearson correlation coefficient = 0.725, $p < 0.001$, AD Pearson correlation coefficient = 0.625, $p <$

0.001), and the parameters from one side of ON were randomly selected in each subject for statistical analysis.

A two-tailed *p*-value of ≤ 0.05 was considered statistically significant, and this was represented as a gray shaded area in the figures. The Pearson correlation coefficient was used to determine the correlation between diffusion measures and age. Additionally, the Jonckheere-Terpstra test was adopted to explore significant trends in diffusion measures among the four age subgroups. A two-sample t-test was used to test for sex-related differences in diffusion measures. Therefore, we performed multiple linear regression analysis to adjust for potentially confounding effects.

Results

Basic Demographics of Study Population

The man age of all subjects was 74.5 ± 8.2 years (range: 55.8 - 95.4) and 58.3% of them (n = 77) were female. The total study population was divided into four age subgroups: (i) 55–65 years, mean age = 61.7 ± 2.6 years, n = 10, 7 females (70.0 %); (ii) 65–75 years, mean age = 69.3 ± 2.7 years, n = 62, 44 females (71.0 %); (iii) 75–85 years, mean age = 79.3 ± 3.1 years, n = 42, 20 females (47.6 %); (iv) 85-95 years, mean age = 88.5 ± 2.8 years, n = 18, 6 females (33.3 %). In this study population, the female participants were significantly younger than the male participants (male vs. female, 77.1 ± 8.3 vs. 72.7 ± 7.7 years, $p = 0.002$). In other words, the older age subgroup had a higher proportion of male participants (linear-by-linear association test, $p = 0.002$).

Diffusion Properties of Total Subjects

The mean FA of the entire intraorbital ON was 0.346 ± 0.078, and the mean MD was 1.266 ± 0.196 $\mu m^2/s$. The mean RD was 1.009 ± 0.195 $\mu m^2/s$, and the mean AD was 1.764 ± 0.210 $\mu m^2/s$.

The diffusion properties along the ON length are summarized with curve graphs in Figure 7. FA gradually increased from 0.250 to 0.404 toward the orbital apex. Meanwhile, MD decreased from 1.529 to 1.121 $\mu m^2/s$. RD and AD also decreased from 1.323 to 0.851 $\mu m^2/s$, and from 1.950 to 1.659 $\mu m^2/s$, respectively.

Figure 7. Averaged tract profiles for the optic nerves of total participants. The graph shows the means (line) and the standard deviations (shaded boundary) of the diffusion parameters of each node of the optic nerve. (A) Fractional anisotropy gradually increased from 0.250 to 0.404, whereas the (B) mean diffusivity decreased from 1.529 to 1.121 $\mu m^2/s$ toward the orbital apex toward the orbital apex. (C) Radial diffusivity also decreased from 1.323 to 0.851 $\mu m^2/s$, and (D) axial diffusivity decreased from 1.950 to 1.659 $\mu m^2/s$.

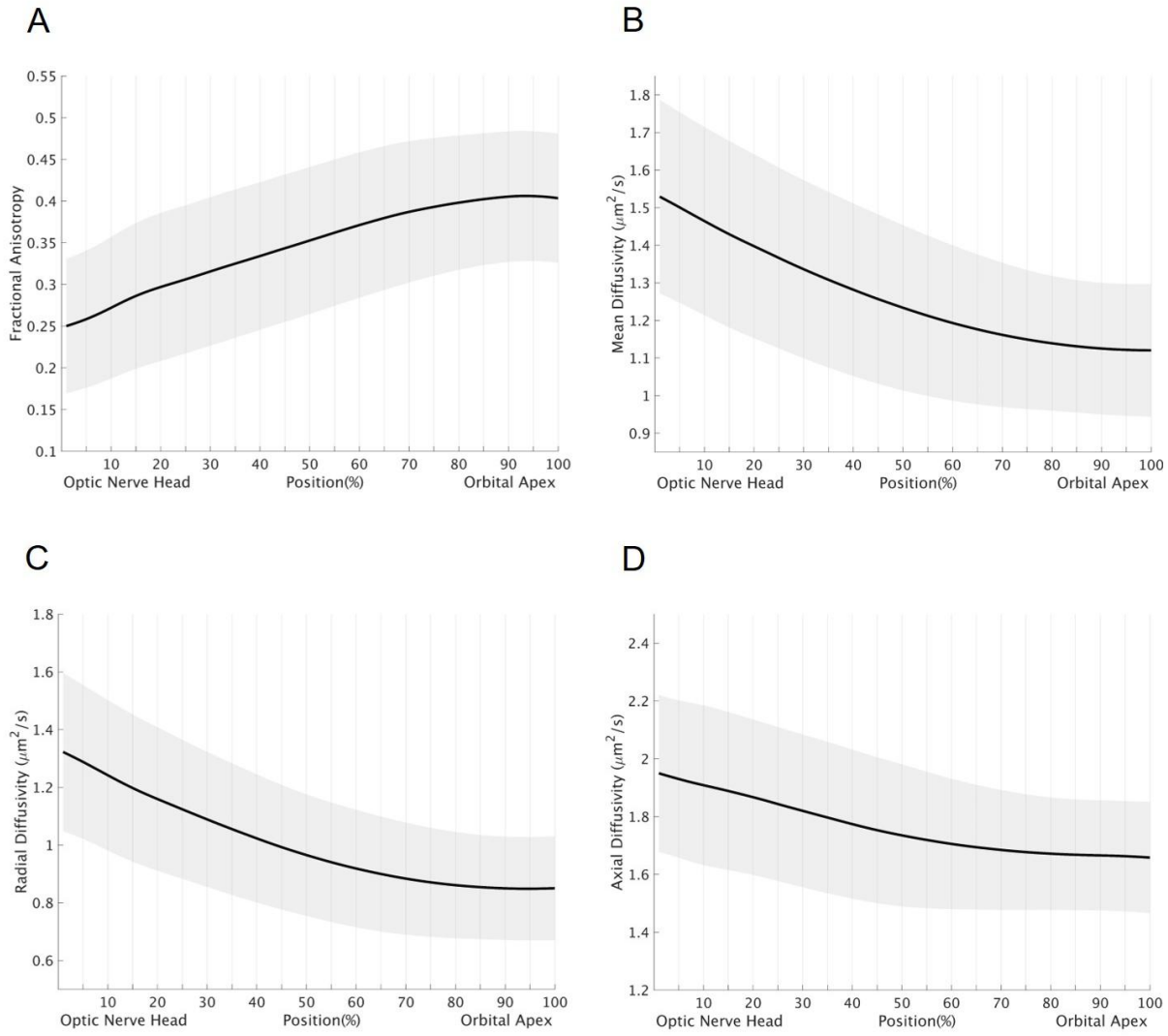

Age-related Changes of Diffusion Properties

FA of the entire intraorbital ON were negatively correlated with age, whereas MD and RD showed a positive correlation (FA with age, Pearson's r = -0.367, $p < 0.001$; MD with age, Pearson's r = 0.162, $p = 0.032$; RD with age, Pearson's r = 0.235, $p = 0007$). However, AD had no significant correlation with age (Pearson's r = -0.025, $p = 0.776$)

The correlation test for each longitudinal position of ON showed a significant negative correlation between FA and age for all 20 nodes, whereas MD had a significant positive correlation with age for the 12 central nodes (60%). RD also showed a significant positive correlation with age in all nodes except for the first node (95%). AD was not correlated with age in the analysis for each node. (Table 2)

Table 2. Data of Pearson's correlation test showing the correlation between age and (A) fractional anisotropy, (B) mean diffusivity, (C) radial diffusivity, and (D) axial diffusivity of each node of optic nerve.

(A)

Node[a]	Fractional anisotropy	
	Correlation coefficient	*p*-value
1	-0.252	**< 0.001**
2	-0.271	**< 0.001**
3	-0.290	**< 0.001**
4	-0.301	**< 0.001**
5	-0.316	**< 0.001**
6	-0.329	**< 0.001**
7	-0.336	**< 0.001**
8	-0.343	**< 0.001**
9	-0.351	**< 0.001**
10	-0.359	**< 0.001**
11	-0.366	**< 0.001**
12	-0.369	**< 0.001**
13	-0.365	**< 0.001**
14	-0.361	**< 0.001**
15	-0.355	**< 0.001**
16	-0.350	**< 0.001**
17	-0.351	**< 0.001**
18	-0.350	**< 0.001**
19	-0.347	**< 0.001**
20	-0.346	**< 0.001**

[a]The nodes of each optic nerve were numbered from the optic nerve head to the orbital apex.
The numbers in bold indicate statistically significant correlations.

(B)

Node[a]	Mean diffusivity ($\mu m^2/s$)	
	Correlation coefficient	*p*-value
1	0.106	0.112
2	0.118	0.090
3	0.130	0.069
4	0.143	0.051
5	0.153	**0.040**
6	0.159	**0.035**
7	0.160	**0.034**
8	0.163	**0.031**
9	0.169	**0.026**
10	0.175	**0.022**
11	0.179	**0.020**
12	0.180	**0.020**
13	0.177	**0.021**
14	0.170	**0.026**
15	0.159	**0.034**
16	0.145	**0.049**
17	0.130	0.069
18	0.114	0.096
19	0.101	0.124
20	0.090	0.151

[a]The nodes of each optic nerve were numbered from the optic nerve head to the orbital apex.
The numbers in bold indicate statistically significant correlations.

(C)

Node[a]	Radial diffusivity ($\mu m^2/s$)	
	Correlation coefficient	*p*-value
1	0.167	0.055
2	0.175	**0.045**
3	0.181	**0.038**
4	0.190	**0.029**
5	0.200	**0.022**
6	0.212	**0.015**
7	0.224	**0.010**
8	0.234	**0.007**
9	0.243	**0.005**
10	0.248	**0.004**
11	0.246	**0.004**
12	0.240	**0.006**
13	0.232	**0.007**
14	0.224	**0.010**
15	0.216	**0.013**
16	0.210	**0.015**
17	0.207	**0.017**
18	0.203	**0.019**
19	0.198	**0.023**
20	0.194	**0.023**

[a]The nodes of each optic nerve were numbered from the optic nerve head to the orbital apex.
The numbers in bold indicate statistically significant correlations.

(D)

Node[a]	Axial diffusivity ($\mu m^2/s$)	
	Correlation coefficient	*p*-value
1	-0.044	0.967
2	-0.013	0.878
3	-0.018	0.836
4	-0.013	0.880
5	-0.010	0.913
6	-0.007	0.939
7	-0.003	0.975
8	0.001	0.989
9	0.005	0.958
10	0.007	0.935
11	0.007	0.933
12	0.002	0.983
13	-0.10	0.911
14	-0.028	0.747
15	-0.046	0.598
16	-0.059	0.505
17	-0.070	0.425
18	-0.080	0.362
19	-0.086	0.325
20	-0.090	0.305

[a]The nodes of each optic nerve were numbered from the optic nerve head to the orbital apex.

The results of the subgroup analysis using the Jonckheere-Terpstra test were comparable to those of the correlation test. (Figure 8) The subgroup analysis showed that the older participants had lower FA and higher RD across the entire ON. MD also significantly decreased with increasing age of participants in the subgroups in forth to nineteenth nodes (80%) from the ON head to the orbital apex. AD had no significant changes according to aging.

Figure 8. Diffusion parameters in age-subgroups along the optic nerve pathway. The curved line shows the means of the diffusion parameters of each subgroup, and the shaded areas indicate the statistically significant correlation between the diffusion parameters and age demonstrated by the Jonckheere-Terpstra test. (A) Fractional anisotropy shows a negative correlation with age along entire optic nerve pathways, whereas the (B) mean diffusivity has a positive correlation with age in 80% of the optic nerve pathways. (C) Radial diffusivity is positively correlated with age in all nodes and (D) axial diffusivity has no significant correlation with age in subgroup analysis.

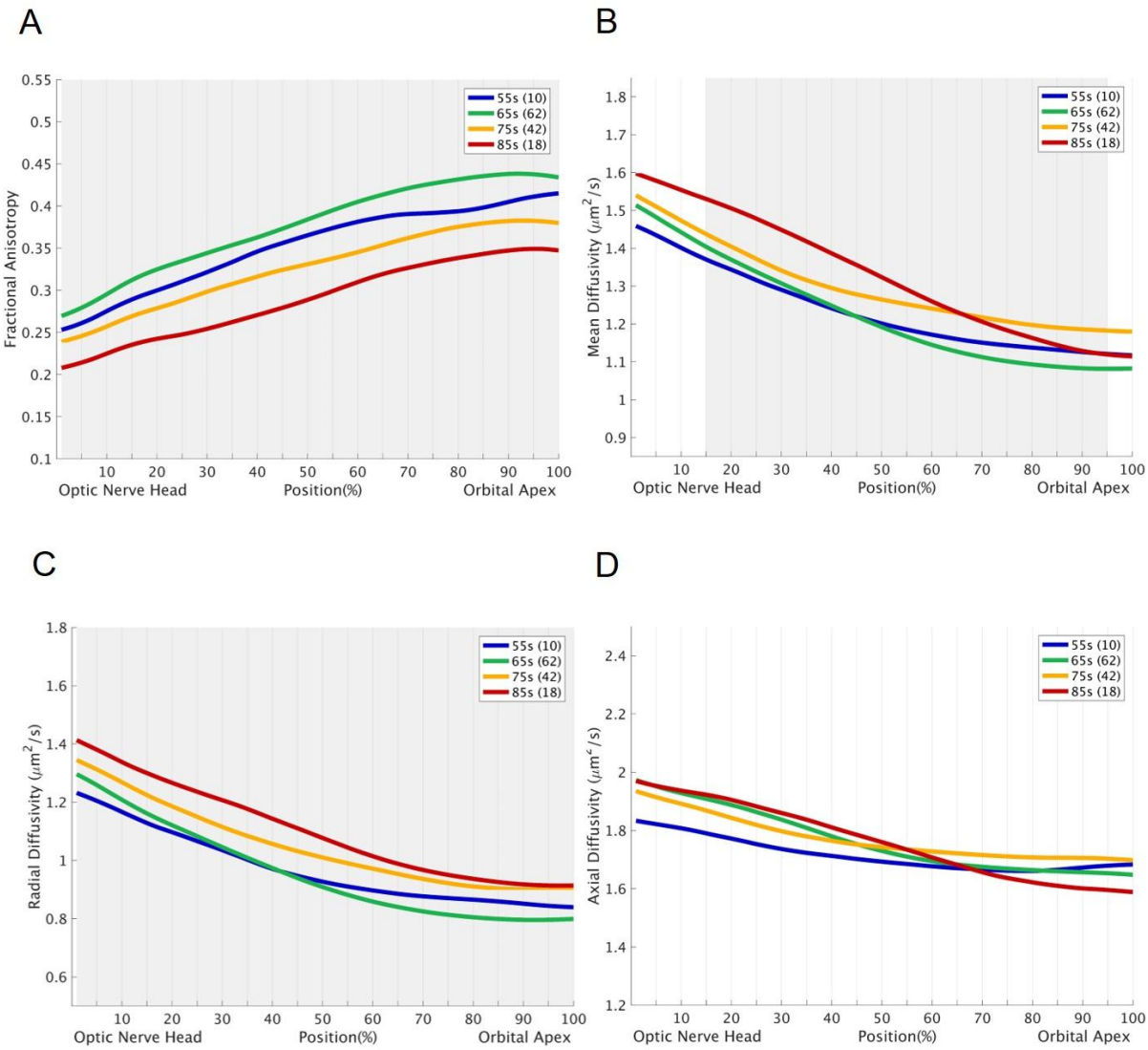

Sex-related Differences in Diffusion Properties

The mean FA, MD, and RD of the entire intraorbital ON of the male and female subjects were significantly different; female subjects had higher FA and lower MD and RD (FA in male vs. female, 0.309 ± 0.065 vs. 0.372 ± 0.075, $p < 0.001$; MD in male vs. female, 1.330 ± 0.163 vs. 1.221 ± 0.204 $\mu m^2/s$, $p = 0.001$, RD in male vs. female, 1.084 ± 0.151 vs. 0.955 ± 0.206 $\mu m^2/s$, $p = 0.002$). The

difference in the mean AD between male and female subjects was not statistically significant (AD in male vs. female, 1.790 ± 0.193 vs. 1.745 ± 0.220 μm^2/s, p = 0.087).

Furthermore, FA showed significant sex-related differences in all 20 nodes of ON. Significant difference was also found for MD in the anterior 19 nodes (95%), RD in the anterior 11 nodes (55%), and AD in the only 2 nodes (10%). (Figure 9)

Figure 9. Sex-related differences in diffusion parameters. The curved line shows the means of the diffusion parameters stratified by sex, and the shaded areas indicate a statistically significant correlation between the diffusion parameters and sex. (A) Females have higher values of fractional anisotropy along the entire optic nerve and (B) lower mean diffusivity in the anterior 95% of the optic nerve. (C) The mean radial diffusivity is higher in the male group in the anterior 55% of the optic nerve. (D) The sex-related difference in axial diffusivity is significant only in the anterior 10% of the optic nerve.

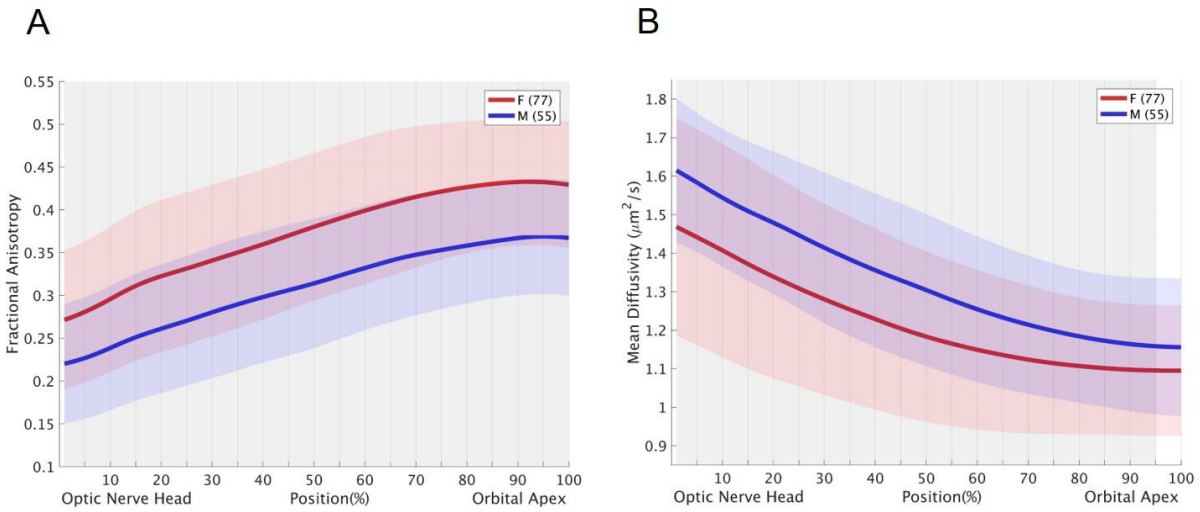

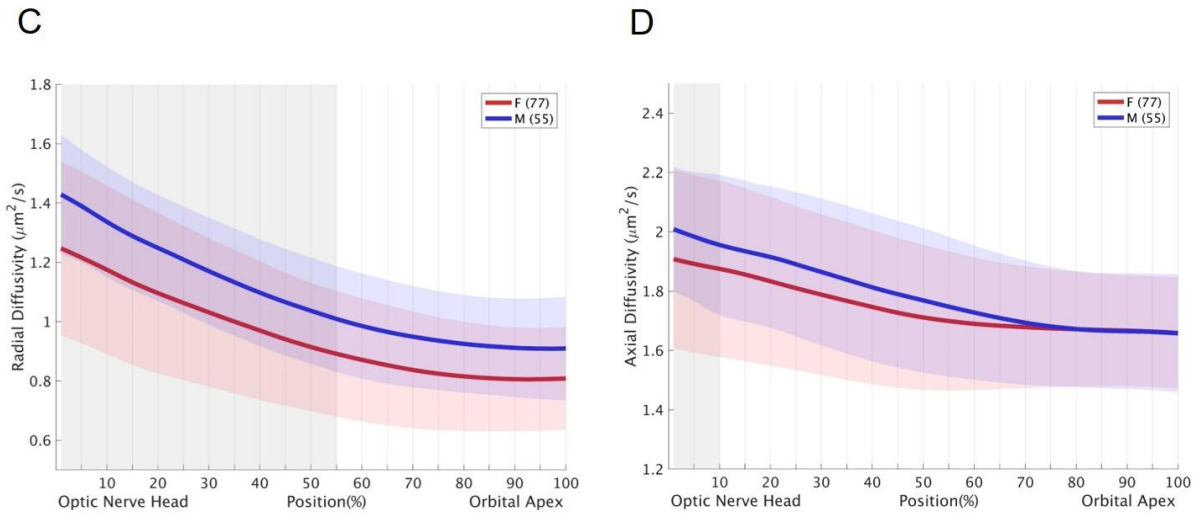

Multiple Linear Regression Analysis for Diffusion Properties

We performed multiple linear regression analysis to adjust for potentially confounding effects. In multiple linear regression analysis, FAs of all 20 nodes, as well as the entire intraorbital ON, showed significant correlation with both age and sex. However, MD did not show a significant correlation with age. MDs of the anterior 19 nodes (95%) and that of the entire ON were significantly correlated with sex. Female had significantly lower RD in all nodes of the intraorbital ON, and RD was positively correlated with age in a fourth of the ON. (Table 3) Meanwhile, no variable was entered into the multiple linear regression model by a stepwise entry for AD except for the first node; AD showed significant correlation with sex only in the first node of the ON (standardized coefficient = -0.183, $p = 0.035$, adjusted $R^2 = 0.026$)

Table 3. Data for multiple linear regression model for (A) fractional anisotropy, (B) mean diffusivity and (C) radial diffusivity of the entire optic nerve and each node of the optic nerve.

(A)

Node[a]	Age		Sex[b]		Adjusted R^2
	Standardized coefficient	*p*-value	Standardized coefficient	*p*-value	
Total	-0.280	**0.001**	0.327	**< 0.001**	0.222
1	-0.181	**0.035**	0.265	**0.002**	0.115
2	-0.198	**0.021**	0.273	**0.002**	0.129
3	-0.227	**0.008**	0.280	**0.001**	0.150
4	-0.243	**0.004**	0.275	**0.001**	0.158
5	-0.239	**0.004**	0.296	**0.001**	0.169
6	-0.258	**0.002**	0.268	**0.002**	0.163
7	-0.266	**0.002**	0.264	**0.002**	0.165
8	-0.272	**0.001**	0.266	**0.002**	0.171
9	-0.278	**0.001**	0.276	**0.001**	0.181
10	-0.282	**0.001**	0.289	**0.001**	0.194
11	-0.287	**0.001**	0.297	**< 0.001**	0.204
12	-0.288	**< 0.001**	0.301	**< 0.001**	0.208
13	-0.283	**0.001**	0.306	**< 0.001**	0.208
14	-0.277	**0.001**	0.317	**< 0.001**	0.212
15	-0.266	**0.001**	0.334	**< 0.001**	0.218
16	-0.257	**0.002**	0.349	**< 0.001**	0.224
17	-0.257	**0.002**	0.352	**< 0.001**	0.226
18	-0.258	**0.002**	0.345	**< 0.001**	0.221
19	-0.258	**0.002**	0.334	**< 0.001**	0.212
20	-0.259	**0.002**	0.327	**< 0.001**	0.207

[a]The nodes of the optic nerve were numbered from the head to the orbital apex.
[b]The reference group is male.
The numbers in bold indicate statistically significant correlations.

(B)

Node[a]	Age		Sex[b]		Adjusted R^2
	Standardized coefficient	*p*-value	Standardized coefficient	*p*-value	
Total	N/A	0.281	-0.277	**0.001**	0.070
1	N/A	0.696	-0.280	**0.001**	0.071
2	N/A	0.585	-0.274	**0.001**	0.068
3	N/A	0.476	-0.269	**0.002**	0.065
4	N/A	0.395	-0.277	**0.001**	0.069
5	N/A	0.339	-0.284	**0.001**	0.073
6	N/A	0.304	-0.281	**0.001**	0.072
7	N/A	0.292	-0.277	**0.001**	0.069
8	N/A	0.266	-0.273	**0.002**	0.067
9	N/A	0.237	-0.273	**0.002**	0.067
10	N/A	0.207	-0.273	**0.002**	0.067
11	N/A	0.184	-0.266	**0.002**	0.063
12	N/A	0.171	-0.254	**0.003**	0.058
13	N/A	0.174	-0.244	**0.005**	0.052
14	N/A	0.192	-0.235	**0.007**	0.048
15	N/A	0.232	-0.226	**0.009**	0.044
16	N/A	0.288	-0.214	**0.014**	0.038
17	N/A	0.359	-0.201	**0.021**	0.033
18	N/A	0.442	-0.188	**0.031**	0.028
19	N/A	0.519	-0.177	**0.042**	0.024

[a]The nodes of the optic nerve were numbered from its head to the orbital apex.
[b]The reference group is male.
The numbers in bold indicate statistically significant correlations.
No variable was entered into the multiple linear regression model by a stepwise entry for mean diffusivity of the last nodes.

(C)

Node[a]	Age		Sex[b]		Adjusted R^2
	Standardized coefficient	*p*-value	Standardized coefficient	*p*-value	
Total	N/A	0.064	-0.327	**< 0.001**	0.100
1	N/A	0.316	-0.326	**< 0.001**	0.100
2	N/A	0.262	-0.318	**< 0.001**	0.094
3	N/A	0.215	-0.303	**< 0.001**	0.085
4	N/A	0.175	-0.302	**< 0.001**	0.084
5	N/A	0.140	-0.302	**< 0.001**	0.084
6	N/A	0.100	-0.296	**0.001**	0.081
7	N/A	0.069	-0.290	**0.001**	0.077
8	0.171	**0.050**	-0.239	**0.006**	0.094
9	0.180	**0.039**	-0.236	**0.007**	0.097
10	0.184	**0.034**	-0.238	**0.007**	0.100
11	0.184	**0.035**	-0.234	**0.007**	0.098
12	0.179	**0.040**	-0.230	**0.009**	0.093
13	N/A	0.051	-0.277	**0.001**	0.069
14	N/A	0.067	-0.282	**0.001**	0.072
15	N/A	0.085	-0.290	**0.001**	0.077
16	N/A	0.101	-0.293	**0.001**	0.079
17	N/A	0.112	-0.294	**0.001**	0.080
18	N/A	0.121	-0.292	**0.001**	0.078
19	N/A	0.131	-0.284	**0.001**	0.074
20	N/A	0.139	-0.277	**0.001**	0.030

[a]The nodes of the optic nerve were numbered from its head to the orbital apex.
[b]The reference group is male.
The numbers in bold indicate statistically significant correlations.

Discussion

In this study, we determined the normal values of diffusion parameters of the intraorbital ON using dMRI probabilistic tractography in cognitively normal controls of the ADNI3 database. We found that FA increased, and MD, RD and AD decreased toward the orbital apex. Furthermore, FA had a negative correlation with age, whereas MD showed no significant change with age. RD was correlated with aging in the central part of the intraorbital ON. Females had higher FA and lower MD and RD than males.

Diffusion Properties along the Intraorbital Optic Nerve

We conducted the present study using dMRI tractography. Thus, we investigated the diffusion properties of the entire intraorbital ON, and not for the limited portions of ON as ROIs, which is one of the greatest strengths of this study. We found that the posterior part of the intraorbital ON showed higher FA and lower MD, RD, and AD than the anterior part.

The change in diffusion parameters stratified by the longitudinal position of the ON is comparable with the results of a previous structural study that used MRI and histology.[43] There was a significant decrease in intraorbital ON diameter from 3.99 mm to 3.50 mm along its length, reflecting a reduction in connective tissues. In other words, the ratio of nervous to connective tissues increases, and nerve fibers become more compact with progression from the anterior to the posterior. Longitudinal structural changes along the intraorbital ON may contribute to the decrease in diffusivity and the increase in FA.

Age-related Changes of Diffusion Properties

Age-related ON changes in various animals have been previously reported.[44-49] In summary, age-related changes may be classified into four: (i) axonal changes, (ii) myelin abnormalities, (iii) changes in neuroglial cells, and (iv) connective tissue thickening. Aging axons undergo various degenerative changes, and the number of nerve fibers decreases with aging. Meanwhile, the volume of aging axons and the thickness of the entire ON fiber increase. Myelin sheaths also become thicker as the thickness of the axons increases. In addition, morphological alterations of myelin sheaths, including ballooning, widening of sheath lamellae, partial loss, and demyelination have been observed. Microglia are commonly observed among degenerating axons, and the number of astrocytes also increases. They undergo hypertrophy, and their processes occupy space vacated by degenerated nerve fibers. Last, aging ONs demonstrate thickening of the trabeculae of connective tissue. In studies involving the human ON, similar changes have been reported.[50-52]

In the current study, FA decreased with age. Age-related changes in the microstructure of the ON contribute to the decrease in FA detected by dMRI. The white matter and cranial nerves, including the ON, consist of bundles of axons, whose membranes and myelin sheaths mainly induce diffusion restriction of water molecules. The direction of maximum diffusivity becomes parallel to the axonal direction, making the diffusion anisotropic.[7, 8] Because the parallel organization of nerve fiber bundles is the basis for diffusion anisotropy and myelin sheaths seem to modulate the amount of anisotropy,[53] the degeneration of axon and myelin sheaths may reduce the anisotropy of the diffusion process. Disintegration caused by the neuroglial cells and connective tissues may also contribute to the decrease in anisotropy.

Interestingly, MD showed no significant correlation with aging in the multiple regression model.

RD in the central part of ON increased with aging, and AD had no significant correlation with age. The age-related changes of ON diffusion parameters in our study are consistent with the previous animal study using DTI for the ON of rhesus monkey.[54] However, the changes in the amount of diffusivity have been various in previous studies for the age-related changes of the white matter in multiple regions although they have consistently reported a decrease in FA.[14]

Because AD tends to be more variable according to pathologic changes, age-related decreases as well as increases in AD have been reported, resulting no net difference, increase, or decrease in MD. In contrast to AD, multiple studies suggested that RD changes is more prominent according to aging,[55-58] and most studies have reported that RD has decreased with increasing age. However, a few studies have revealed that a decrease in AD and MD without a difference in RD.[59, 60] Based on these different patterns of diffusivity changes, several studies have classified the regions of brain according to the specific age-related pathologic change.[59, 60] When applied to this classification, the results from the ON in this study, a decrease in FA accompanied with a mild increase in RD, suggest that the main pathologic changes is the subtle microstructural alterations with predominant demyelination in the ON aging process, which is like the forceps major and superior corona radiata. Further studies are required to answer the question of why the aging process occurs in various ways according to region of the nervous system.

In the meantime, Sun et al. previously reported that there was no obvious age-related difference in diffusion parameters of ON and optic radiation in DTI.[61] In that study, the authors measured the diffusion parameters in ROI at the level of the middle part of intraorbital ON. In addition, they included the healthy subjects aged from 18 to 62 years (mean age = 40.3 ± 12.5 years), who were younger than our study subjects. Therefore, it should be noted that local diffusion properties of the

ON before the seventh decade of life may not show any significant age-related change.

Sex-related Differences in Diffusion Properties

Sun et al. also said that there was no obvious difference in diffusion parameters between female and male subjects, which was conflicting with our results.[61] In the present study, females had higher FA and lower MD and RD than males. Sex-related difference in our results is consistent with the reports by other studies on sex-related differences in ON structure and function. Various studies have previously reported the association of the male sex with thinner retinal nerve fiber layers on OCT,[62-65] whereas the optic disc area is larger in males than in females.[66-68] It means that the axonal density of the intraorbital ON is higher in females than in males. In addition to the structural differences, several differences in visual evoked potentials have been revealed, such as shorter latency and high amplitude in females.[69, 70]

Although any significant interaction between age and sex were not found in the brain white matter, it is highly advisable to consider that sex-related difference could become more prominent due to the difference in the course of ON neurodegeneration between female and male, considering that we analyzed the data from an elderly population.[71] Previously sex-related difference in the brain white matter have been reported in several studies, and the results were varied among those studies due to the discrepancy of age of the study population and regions of brain for analysis.[72-74] The retinal ganglion cells are exposed to light over all one's life, and the intraorbital ON is surrounded with soft tissue such as orbital fat in contrast to the brain tissue in the rock-solid skull.[75] In addition to the damage induced by external environment, retinal gene expression responses to aging has been reported to be sexually divergent.[76] Therefore, sex-related difference in diffusion properties of ON

should be sufficiently consider in an elderly population.

Placement of Region of Interest for the Intraorbital Optic Nerve

In previous studies using tractography for ON analysis in various diseases, the ROIs were placed at the optic chiasm as the ending point.[25, 26] In contrast to these studies, we analyzed the diffusion parameters of only the intraorbital parts of ON. When tractography, involving the intracanalicular and intracranial ON, was performed, the diffusivity along the ON fluctuated. (Figure 10) This implies that the extracted tractography included heterogeneous tract fibers that were not confined to the ON. Compact tissues around the ON in the optic canal and the cranial cavity may make false tracts of the visual pathway.

Figure 10. Tractography from optic disc head to optic chiasm. (A) Optic nerve visualization using diffusion magnetic resonance imaging probabilistic tractography. (B) Tract profile for the optic nerve including fractional anisotropy and mean diffusivity. When tractography, involving the intracanalicular and intracranial optic nerve, is generated, the diffusion properties along the optic nerve has substantial fluctuation.

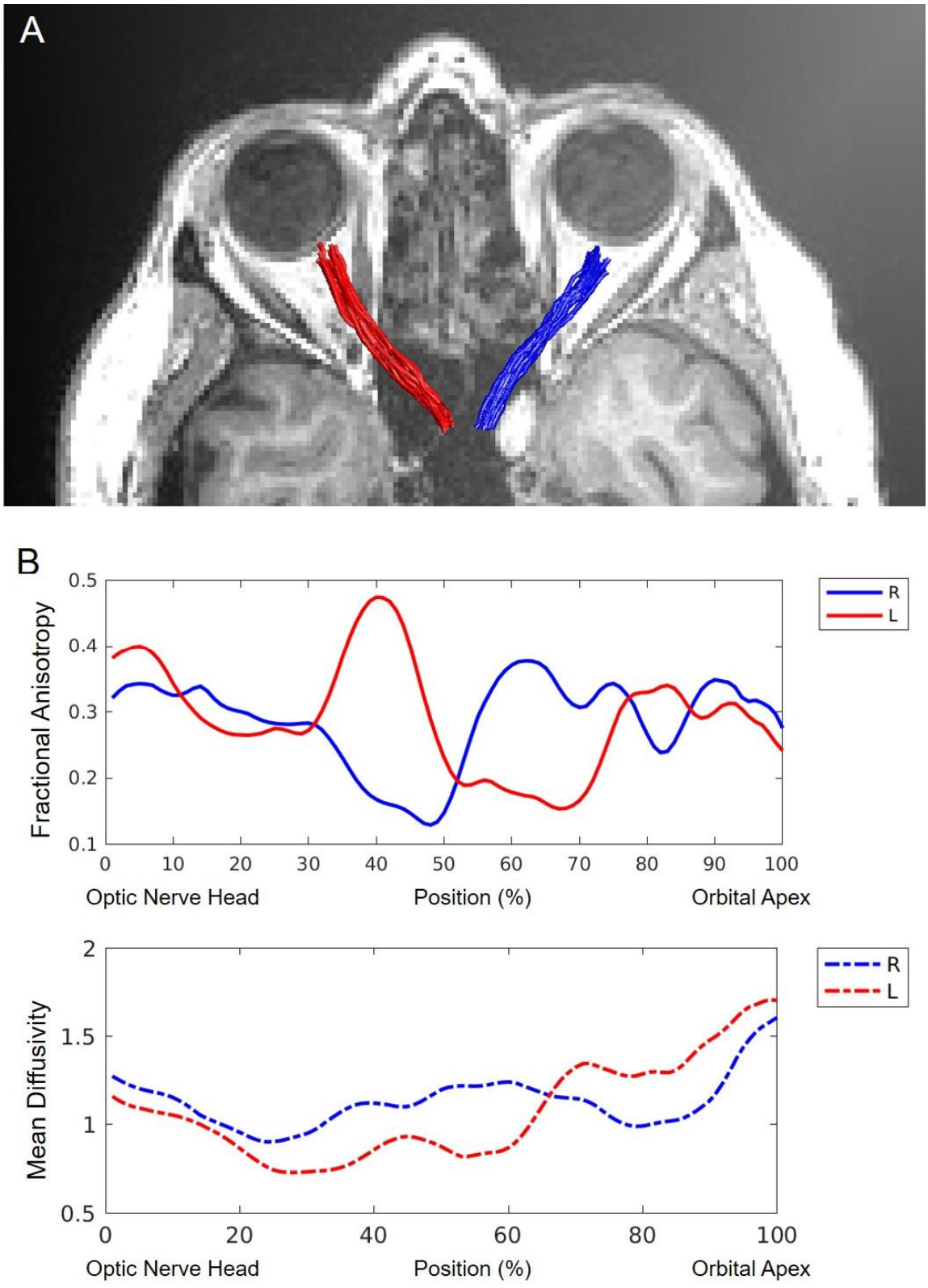
A
B
Fractional Anisotropy
0.5
0.4
0.3
0.2
0.1
0
10
20
30
40
50
60
70
80
90
100
Optic Nerve Head
Position (%)
Orbital Apex
R
L
Mean Diffusivity
2
1.5
1
0.5
0
20
40
60
80
100
Optic Nerve Head
Position (%)
Orbital Apex
R
L

Moreover, the placement of ROIs is important because it can induce significantly different outcomes of the final tractography. In the ADNI3 database, diffusion sequences had image distortions; diffusion scans acquired with opposite phase-encoding directions were not used. As mentioned in the Methods section, we prioritized b0 MR images when the anatomical structures in the T1-weighted and b0 MR images were not completely matched, and the optic chiasm in b0 MR images could not be located in several cases. To reduce errors for ROI placement and perform more accurate tractography, we placed ROIs in the center of the annulus of Zinn, which is a confluence of the extraocular muscles, to facilitate the identification of the ON pathways. Then, we found that all ICC values of diffusion parameters were more than 0.85, which demonstrated excellent reproducibility of the ROI placement for intraorbital ON.[77]

Strengths and Limitations

This study has several limitations that should be addressed. First, the dMRI data used in this study were obtained from the ADNI3. All the subjects with normal cognitive functions in ADNI3 may not have been ophthalmologically normal due to the limited ophthalmologic information of the participants. We randomly selected the parameters from one side in each subject because the measurements between both eyes of the same individual were highly correlated with each other. However, the error could be induced by including eyes with ocular disease. In addition, the ADNI3 data were collected across the United States and Canada and we were able to measure the diffusion parameters of ON only in an elderly population, which may result in lower FA compared to previous studies.[21, 61] Therefore, further studies including subjects with a wide range of ages and various racial

and environmental background are needed for general implication of the reference value for diffusion properties.

Second, the data from ADNI3 are not intended for the analysis of ON. Accordingly, eye movement correction was not applied. In addition, the images acquired from the diffusion protocol suffer from geometric distortions caused by a single phase-encoding direction. Accordingly, a mismatch between the T1-weighted image and b0 MR image was induced. (Figure 11) In this study, we attempted to overcome this limitation by prioritizing b0 MR images when placing the ROIs.

Figure 11. Geometric distortion in diffusion magnetic resonance images. (A, B) When there was a difference between the locations of the ROIs of the T1-weighted image and b0 image, we choose b0 images to locate the ROI. (C, D) Final tractography is well matched with the b0 image rather than the T1-weighted image.

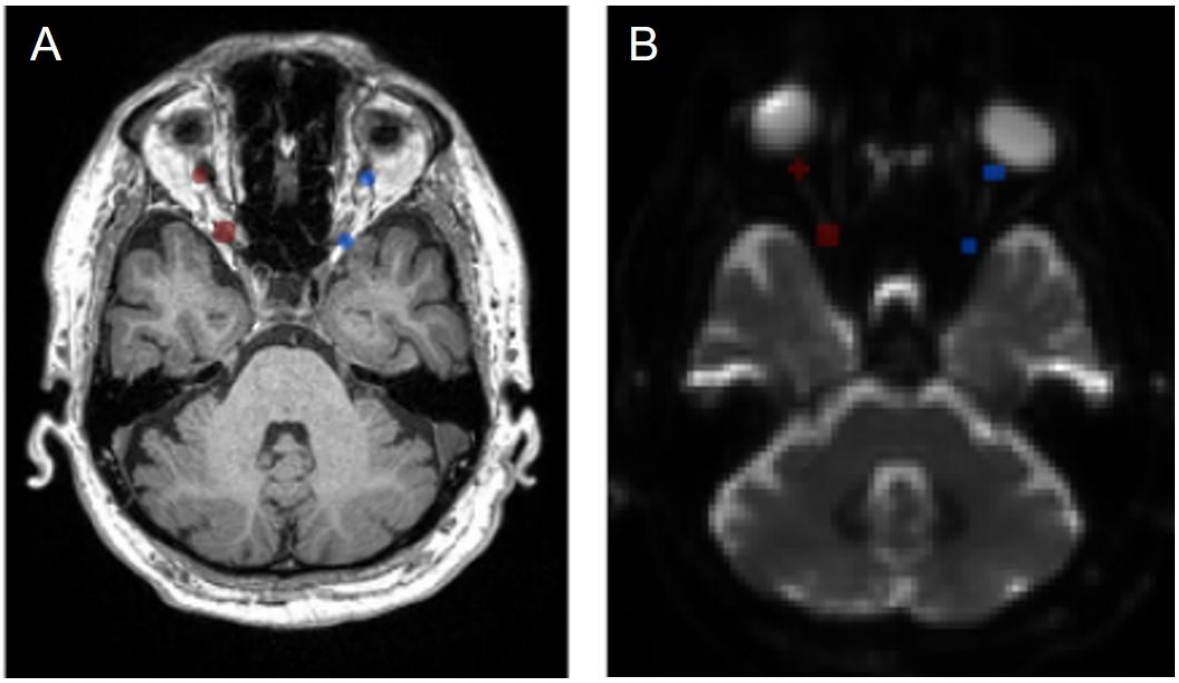

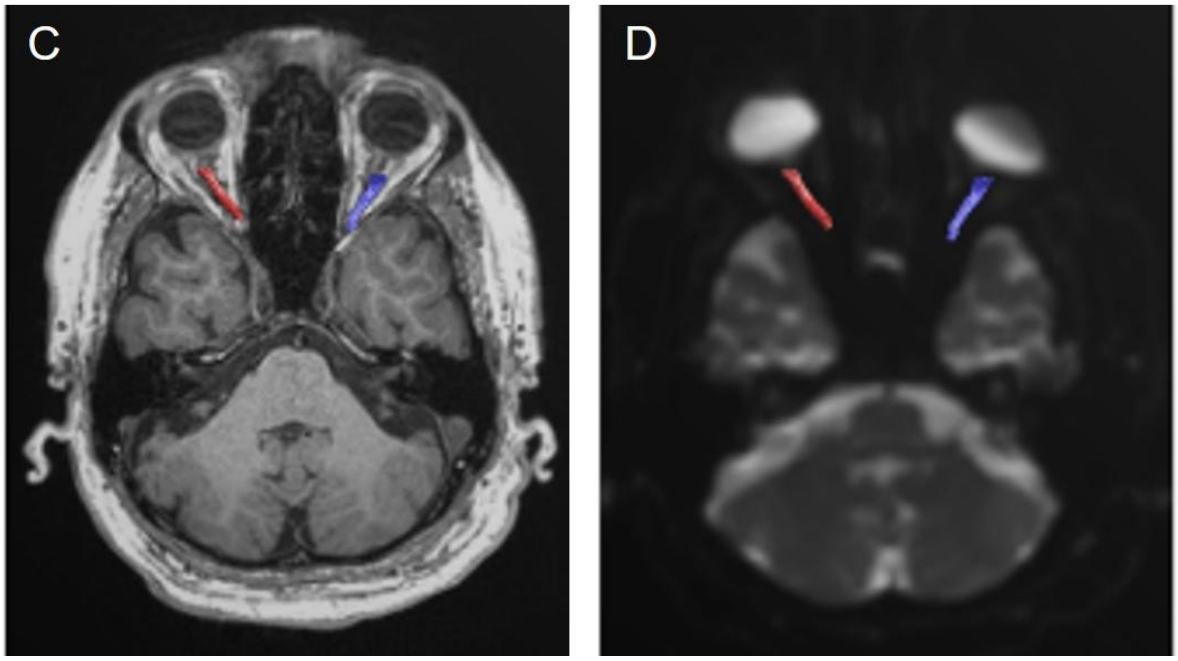

Despite these limitations, to the best of our knowledge, this is the first study to investigate the diffusion properties of ON and suggest reference values of diffusion parameters using large-scale, multi-site neuroimaging data. This study showed the diffusion properties stratified by age, sex, and longitudinal location of the ON using four diffusion parameters, FA, MD, RD and AD. Moreover, the results from the present analysis correspond well with those of previous studies on the ON structures and functions. This implies that the diffusion parameters along the ON determined using dMRI tractography may substantially reflect the ON microstructure and have clinical usefulness.

Conclusion

In conclusion, we measured the diffusion properties of normal ON using dMRI tractography and evaluated its microstructural characteristics. FA increased, whereas MD, RD and AD reduced toward the orbital apex. FA decreased and RD increased with age. Females had higher FA and lower MD and

RD than males. The differences based on the longitudinal position of the ON, age, and sex should be considered when evaluating the ON using dMRI.

The findings in this study suggested that the diffusion properties in dMRI tractography well represent microstructural changes of ON. Therefore, dMRI can help improve the understanding of the pathophysiologic mechanisms of various ON diseases.

References

1. Kirbas S, Turkyilmaz K, Anlar O, Tufekci A, Durmus M. Retinal nerve fiber layer thickness in patients with Alzheimer disease. J Neuroophthalmol 2013;33:58-61.

2. Yu JG, Feng YF, Xiang Y, et al. Retinal nerve fiber layer thickness changes in Parkinson disease: a meta-analysis. PLoS One 2014;9:e85718.

3. Baumal CR. Clinical applications of optical coherence tomography. Curr Opin Ophthalmol 1999;10:182-188.

4. Paunescu LA, Schuman JS, Price LL, et al. Reproducibility of nerve fiber thickness, macular thickness, and optic nerve head measurements using StratusOCT. Invest Ophthalmol Vis Sci 2004;45:1716-1724.

5. Spaide RF, Koizumi H, Pozzoni MC. Enhanced depth imaging spectral-domain optical coherence tomography. Am J Ophthalmol 2008;146:496-500.

6. Laviers H, Zambarakji H. Enhanced depth imaging-OCT of the choroid: a review of the current literature. Graefes Arch Clin Exp Ophthalmol 2014;252:1871-1883.

7. Moseley ME, Cohen Y, Kucharczyk J, et al. Diffusion-weighted MR imaging of anisotropic water diffusion in cat central nervous system. Radiology 1990;176:439-445.

8. Tanner JE. Self diffusion of water in frog muscle. Biophys J 1979;28:107-116.

9. Jeurissen B, Descoteaux M, Mori S, Leemans A. Diffusion MRI fiber tractography of the brain. NMR Biomed 2019;32:e3785.

10. de Figueiredo EH, Borgonovi AF, Doring TM. Basic concepts of MR imaging, diffusion MR imaging, and diffusion tensor imaging. Magn Reson Imaging Clin N Am 2011;19:1-22.

11. Zhan L, Zhou JY, Wang YL, et al. Comparison of nine tractography algorithms for detecting abnormal structural brain networks in Alzheimer's disease. Front Aging Neurosci 2015;7.

12. Basser PJ, Pierpaoli C. Microstructural and physiological features of tissues elucidated by quantitative-diffusion-tensor MRI. J Magn Reson Ser B 1996;111:209-219.

13. Pierpaoli C, Basser PJ. Toward a quantitative assessment of diffusion anisotropy. Magnet Reson Med 1996;36:893-906.

14. Madden DJ, Bennett IJ, Burzynska A, Potter GG, Chen NK, Song AW. Diffusion tensor imaging of cerebral white matter integrity in cognitive aging. Bba-Mol Basis Dis 2012;1822:386-400.

15. Alexander AL, Lee JE, Lazar M, Field AS. Diffusion tensor imaging of the brain. Neurotherapeutics 2007;4:316-329.

16. Song SK, Sun SW, Ju WK, Lin SJ, Cross AH, Neufeld AH. Diffusion tensor imaging detects and differentiates axon and myelin degeneration in mouse optic nerve after retinal ischemia. Neuroimage 2003;20:1714-1722.

17. Song SK, Yoshino J, Le TQ, et al. Demyelination increases radial diffusivity in corpus callosum of mouse brain. Neuroimage 2005;26:132-140.

18. Winklewski PJ, Sabisz A, Naumczyk P, Jodzio K, Szurowska E, Szarmach A. Understanding the Physiopathology Behind Axial and Radial Diffusivity Changes - What Do we Know? Frontiers in Neurology 2018;9.

19. Wang MY, Wu K, Xu JM, et al. Quantitative 3-T diffusion tensor imaging in detecting optic nerve degeneration in patients with glaucoma: association with retinal nerve fiber layer thickness and clinical severity. Neuroradiology 2013;55:493-498.

20. Smith SA, Williams ZR, Ratchford JN, et al. Diffusion tensor imaging of the optic nerve in multiple sclerosis: association with retinal damage and visual disability. AJNR Am J Neuroradiol 2011;32:1662-1668.

21. Zhang QJ, Wang D, Bai ZL, Ren BC, Li XH. Diffusion tensor imaging of optic nerve and optic

radiation in primary chronic angle-closure glaucoma using 3T magnetic resonance imaging. Int J Ophthalmol-Chi 2015;8:975-979.

22. Andersson JL, Skare S, Ashburner J. How to correct susceptibility distortions in spin-echo echo-planar images: application to diffusion tensor imaging. Neuroimage 2003;20:870-888.

23. Mori S, van Zijl PC. Fiber tracking: principles and strategies - a technical review. NMR Biomed 2002;15:468-480.

24. Ciccarelli O, Catani M, Johansen-Berg H, Clark C, Thompson A. Diffusion-based tractography in neurological disorders: concepts, applications, and future developments. Lancet Neurol 2008;7:715-727.

25. Allen B, Schmitt MA, Kushner BJ, Rokers B. Retinothalamic White Matter Abnormalities in Amblyopia. Invest Ophthalmol Vis Sci 2018;59:921-929.

26. Miller N, Liu Y, Krivochenitser R, Rokers B. Linking neural and clinical measures of glaucoma with diffusion magnetic resonance imaging (dMRI). PLoS One 2019;14:e0217011.

27. Veitch DP, Weiner MW, Aisen PS, et al. Understanding disease progression and improving Alzheimer's disease clinical trials: Recent highlights from the Alzheimer's Disease Neuroimaging Initiative. Alzheimers Dement 2019;15:106-152.

28. Zavaliangos-Petropulu A, Nir TM, Thomopoulos SI, et al. Diffusion MRI Indices and Their Relation to Cognitive Impairment in Brain Aging: The Updated Multi-protocol Approach in ADNI3. Front Neuroinform 2019;13:2.

29. Alexander AL, Hasan KM, Lazar M, Tsuruda JS, Parker DL. Analysis of partial volume effects in diffusion-tensor MRI. Magn Reson Med 2001;45:770-780.

30. Cercignani M, Bammer R, Sormani MP, Fazekas F, Filippi M. Inter-sequence and inter-imaging unit variability of diffusion tensor MR imaging histogram-derived metrics of the brain in

healthy volunteers. AJNR Am J Neuroradiol 2003;24:638-643.

31. Zhu T, Hu R, Qiu X, et al. Quantification of accuracy and precision of multi-center DTI measurements: a diffusion phantom and human brain study. Neuroimage 2011;56:1398-1411.

32. Zhan L, Leow AD, Jahanshad N, et al. How does angular resolution affect diffusion imaging measures? neuroimage 2010;49:1357-1371.

33. Kellner E, Dhital B, Kiselev VG, Reisert M. Gibbs-ringing artifact removal based on local subvoxel-shifts. Magn Reson Med 2016;76:1574-1581.

34. Tournier JD, Smith R, Raffelt D, et al. MRtrix3: A fast, flexible and open software framework for medical image processing and visualisation. Neuroimage 2019;202:116137.

35. Tustison NJ, Avants BB, Cook PA, et al. N4ITK: improved N3 bias correction. IEEE Trans Med Imaging 2010;29:1310-1320.

36. Veraart J, Fieremans E, Novikov DS. Diffusion MRI Noise Mapping Using Random Matrix Theory. Magnetic Resonance in Medicine 2016;76:1582-1593.

37. Veraart J, Novikov DS, Christiaens D, Ades-Aron B, Sijbers J, Fieremans E. Denoising of diffusion MRI using random matrix theory. Neuroimage 2016;142:384-396.

38. Rohde GK, Barnett AS, Basser PJ, Marenco S, Pierpaoli C. Comprehensive approach for correction of motion and distortion in diffusion-weighted MRI. Magn Reson Med 2004;51:103-114.

39. Sherbondy AJ, Dougherty RF, Ben-Shachar M, Napel S, Wandell BA. ConTrack: Finding the most likely pathways between brain regions using diffusion tractography. J Vision 2008;8.

40. Takemura H, Ogawa S, Mezer AA, et al. Diffusivity and quantitative T1 profile of human visual white matter tracts after retinal ganglion cell damage. Neuroimage-Clin 2019;23.

41. Basser PJ. Inferring microstructural features and the physiological state of tissues from diffusion-weighted images. NMR Biomed 1995;8:333-344.

42. Yeatman JD, Dougherty RF, Myall NJ, Wandell BA, Feldman HM. Tract profiles of white matter properties: automating fiber-tract quantification. PLoS One 2012;7:e49790.

43. Karim S, Clark RA, Poukens V, Demer JL. Demonstration of systematic variation in human intraorbital optic nerve size by quantitative magnetic resonance imaging and histology. Invest Ophthalmol Vis Sci 2004;45:1047-1051.

44. Stahon KE, Bastian C, Griffith S, Kidd GJ, Brunet S, Baltan S. Age-Related Changes in Axonal and Mitochondrial Ultrastructure and Function in White Matter. J Neurosci 2016;36:9990-10001.

45. Cavallotti D, Cavallotti C, Pescosolido N, Iannetti GD, Pacella E. A morphometric study of age changes in the rat optic nerve. Ophthalmologica 2001;215:366-371.

46. Yassa HD. Age-related changes in the optic nerve of Sprague-Dawley rats: an ultrastructural and immunohistochemical study. Acta Histochem 2014;116:1085-1095.

47. Sandell JH, Peters A. Effects of age on nerve fibers in the rhesus monkey optic nerve. J Comp Neurol 2001;429:541-553.

48. Sandell JH, Peters A. Effects of age on the glial cells in the rhesus monkey optic nerve. J Comp Neurol 2002;445:13-28.

49. Attia H, Taha M, Abdellatif A. Effects of aging on the myelination of the optic nerve in rats. Int J Neurosci 2019;129:320-324.

50. Johnson BM, Miao M, Sadun AA. Age-Related Decline of Human Optic-Nerve Axon Populations. Age 1987;10:5-9.

51. Balazsi AG, Rootman J, Drance SM, Schulzer M, Douglas GR. The Effect of Age on the Nerve-Fiber Population of the Human Optic-Nerve. Am J Ophthalmol 1984;97:760-766.

52. Dolman CL, Mccormick AQ, Drance SM. Aging of the Optic-Nerve. Arch Ophthalmol-Chic 1980;98:2053-2058.

53. Beaulieu C, Allen PS. Determinants of anisotropic water diffusion in nerves. Magn Reson Med 1994;31:394-400.

54. Yan Y, Li L, Preuss TM, Hu X, Herndon JG, Zhang X. In vivo evaluation of optic nerve aging in adult rhesus monkey by diffusion tensor imaging. Quant Imaging Med Surg 2014;4:43-49.

55. Davis SW, Dennis NA, Buchler NG, White LE, Madden DJ, Cabeza R. Assessing the effects of age on long white matter tracts using diffusion tensor tractography. Neuroimage 2009;46:530-541.

56. Madden DJ, Spaniol J, Costello MC, et al. Cerebral White Matter Integrity Mediates Adult Age Differences in Cognitive Performance. J Cognitive Neurosci 2009;21:289-302.

57. Bhagat YA, Beaulieu C. Diffusion anisotropy in subcortical white matter and cortical gray matter: Changes with aging and the role of CSF-suppression. Journal of Magnetic Resonance Imaging 2004;20:216-227.

58. Zhang Y, Du AT, Hayasaka S, et al. Patterns of age-related water diffusion changes in human brain by concordance and discordance analysis. Neurobiol Aging 2010;31:1991-2001.

59. Bennett IJ, Madden DJ, Vaidya CJ, Howard DV, Howard JH. Age-Related Differences in Multiple Measures of White Matter Integrity: A Diffusion Tensor Imaging Study of Healthy Aging. Hum Brain Mapp 2010;31:378-390.

60. Burzynska AZ, Preuschhof C, Backman L, et al. Age-related differences in white matter microstructure: Region-specific patterns of diffusivity. Neuroimage 2010;49:2104-2112.

61. Sun HH, Wang D, Zhang QJ, Bai ZL, He P. Magnetic resonance diffusion tensor imaging of optic nerve and optic radiation in healthy adults at 3T. Int J Ophthalmol-Chi 2013;6:868-872.

62. Wang CY, Zheng YF, Liu B, et al. Retinal Nerve Fiber Layer Thickness in Children: The Gobi Desert Children Eye Study. Invest Ophthalmol Vis Sci 2018;59:5285-5291.

63. Li D, Rauscher FG, Choi EY, et al. Sex-Specific Differences in Circumpapillary Retinal Nerve

Fiber Layer Thickness. Ophthalmology 2020;127:357-368.

64. Khawaja AP, Chan MP, Garway-Heath DF, et al. Associations with retinal nerve fiber layer measures in the EPIC-Norfolk Eye Study. Invest Ophthalmol Vis Sci 2013;54:5028-5034.

65. Wang YX, Pan Z, Zhao L, You QS, Xu L, Jonas JB. Retinal nerve fiber layer thickness. The Beijing Eye Study 2011. PLoS One 2013;8:e66763.

66. Quigley HA, Brown AE, Morrison JD, Drance SM. The size and shape of the optic disc in normal human eyes. Arch Ophthalmol 1990;108:51-57.

67. Bourne RR, Foster PJ, Bunce C, et al. The morphology of the optic nerve head in the Singaporean Chinese population (the Tanjong Pagar study): part 1--Optic nerve head morphology. Br J Ophthalmol 2008;92:303-309.

68. Buteikiene D, Kybartaite-Ziliene A, Kriauciuniene L, Barzdziukas V, Januleviciene I, Paunksnis A. Morphometric parameters of the optic disc in normal and glaucomatous eyes based on time-domain optical coherence tomography image analysis. Medicina (Kaunas) 2017;53:242-252.

69. Sharma R, Joshi S, Singh KD, Kumar A. Visual Evoked Potentials: Normative Values and Gender Differences. J Clin Diagn Res 2015;9:CC12-15.

70. Gregori B, Pro S, Bombelli F, La Riccia M, Accornero N. Vep latency: sex and head size. Clin Neurophysiol 2006;117:1154-1157.

71. Inano S, Takao H, Hayashi N, Abe O, Ohtomo K. Effects of age and gender on white matter integrity. AJNR Am J Neuroradiol 2011;32:2103-2109.

72. Hsu JL, Leemans A, Bai CH, et al. Gender differences and age-related white matter changes of the human brain: a diffusion tensor imaging study. Neuroimage 2008;39:566-577.

73. Simmonds DJ, Hallquist MN, Asato M, Luna B. Developmental stages and sex differences of white matter and behavioral development through adolescence: a longitudinal diffusion tensor imaging

(DTI) study. Neuroimage 2014;92:356-368.

74. Wang Y, Adamson C, Yuan W, et al. Sex differences in white matter development during adolescence: a DTI study. Brain Res 2012;1478:1-15.

75. Youssef PN, Sheibani N, Albert DM. Retinal light toxicity. Eye (Lond) 2011;25:1-14.

76. Du M, Mangold CA, Bixler GV, et al. Retinal gene expression responses to aging are sexually divergent. Mol Vis 2017;23:707-717.

77. Yang JY, Beare R, Wu MH, et al. Optic Radiation Tractography in Pediatric Brain Surgery Applications: A Reliability and Agreement Assessment of the Tractography Method. Front Neurosci 2019;13:1254.

요약

목적: 고령 인구에서 확산자기공명영상 신경섬유추적지도를 이용하여 시신경의 미세구조적 특성을 확인하고 나이 및 성별에 따른 확산 성질의 차이를 규명하고자 한다.

방법: Alzheimer's Disease Neuroimaging Initiative 3 데이터베이스에서 정상 대조군 132명(평균 나이 74.5±8.2세)의 영상 자료를 추출하였다. 확산자기공명영상 신경섬유추적지도를 이용하여 시신경의 분할 비등방도(fractional anisotropy, 이하 FA), 평균 확산도(mean diffusivity, 이하 MD), 방사 확산도(radial diffusivity, 이하 RD)와 향 확산도(axial diffusivity, 이하 AD)를 측정하였다. 또한 확산 계수들과 나이 및 성별 사이의 상관성을 분석하였다. 안와 내 시신경에 대한 신경섬유추적지도를 20개 등거리의 마디로 나누어 네 가지 확산 계수를 측정하였다.

결과: 안와 내 시신경의 평균 FA는 0.346±0.078이었고, 평균 MD는 1.266±0.196 $\mu m^2/s$이었다. 평균 RD는 1.009±0.195 $\mu m^2/s$이었으며, 평균 AD는 1.764±0.210 $\mu m^2/s$이었다. FA는 안와 첨부로 갈수록 0.250에서 0.404로 점진적으로 증가하였으며, MD는 1.529 $\mu m^2/s$에서 1.121 $\mu m^2/s$으로 감소하였다. RD와 AD 역시 각각 1.323 $\mu m^2/s$에서 0.851 μm2/s으로, 1.950 $\mu m^2/s$에서 1.659 $\mu m^2/s$으로 줄어들었다. 다중회귀분석에서, FA는 시신경 전 영역에 걸쳐 나이 및 성별과 관련성을 보였는데, 나이가 적을수록, 그리고 여성일수록 더 높은 FA를 가졌다. MD는 나이와는 유의한 상관성이 없었고, 여성이 19개 마디에서 더 낮은 MD를 나타냈다. 시신경 전 영역에서 여성이 남성에 비해 유의미하게 낮은 RD를 보였고, 중간 25% 구간에서 RD와 나이 양의 상관성을 보였다. AD는 첫 번째 마디에서 성별과의 상관성이 있었으나 이를 제외한 전 영역에서 나이 혹은 성별과의 상관성이 없었다.

결론: 본 연구에서 신경섬유추적지도를 이용하여 안와 내 시신경의 전 길이에 걸쳐 네 가지 확산 계수를 측정할 수 있었다. 나이가 증가함에 따라 FA는 감소하였고, RD는 부분적으로 증가하였다. 여성은 남성에 비해 높은 FA, 낮은 MD와 RD를 나타냈다. 신경섬유추적지도를 이용하여 확인된 시신경의 확산 성질은 시신경의 조직학적 미세 구조를 잘 반영하였다.